Science Advances

AAAS

advances.sciencemag.org/cgi/content/full/3/10/e1700969/DC1

Supplementary Materials for

Jamming and overpacking fuzzy microgels: Deformation, interpenetration, and compression

Gaurasundar M. Conley, Philippe Aebischer, Sofi Nöjd, Peter Schurtenberger, Frank Scheffold

Published 20 October 2017, *Sci. Adv.* **3**, e1700969 (2017)
DOI: 10.1126/sciadv.1700969

The PDF file includes:

Other Supplementary Material for this manuscript includes the following:
(available at advances.sciencemag.org/cgi/content/full/3/10/e1700969/DC1)

movie S1 (.mp4 format). Animated 3D visualization of deformed microgels within a densely packed suspension at 25.6 wt %.

I. STATIC LIGHT SCATTERING CHARACTERIZATION

We measure the form factor $P(q)$ of pNIPAM microgels at 22°C using static light scattering (SLS) using a commercial light scattering goniometer (ALV, Germany) at a wavelength of 532nm. To this end we disperse a small amount of microgels in the same solvent used for dSTORM imaging. Next we compare the experimental data to the fuzzy sphere model by Stieger and coworkers (23) as shown in fig. S1. In the model the form factor is given, in reciprocal space, by that of a homogeneous sphere of radius R multiplied by a Gaussian with characteristic length scale σ, about half the thickness of the fuzzy shell. It has been shown that the total radius is approximately given by $R_{\rm tot} \simeq R_{\rm core} + 2\sigma$ (11, 23, 30). Polydispersity can also be taken account for by assuming a Gaussian distribution of radii as explained in (23).

$$P(q) \propto \left[\frac{R\,q\cos(R\,q) \;\; -\sin(R\,q)}{(R\,q)^3} \exp\left(\frac{-\sigma^2 q^2}{2}\right)\right]^2 \quad \text{(S1)}$$

From a fit to the data we obtain $R \equiv R_{\rm core} = 380\ nm$, $\sigma = 45\ nm$ and a polydispersity of 6 %. This corresponds to an overall size of $R_{\rm tot} \simeq 470\ nm$.

II. CONTOUR OF MICROGEL IMAGES

While at first glance it would appear that the images have well defined smooth edges, upon closer inspection their roughness becomes evident. Since our goal is not to characterize the roughness and limited density of dye-labeling, but to distinguish between round and polygonal shapes and to determine their overall size, we apply the following method. First, the rough contour is determined using a Laplacian of Gaussian edge detection method. Second, we smooth the contour using Fourier descriptors (42), a versatile method in image analysis. An example of this procedure applied to a round and to a faceted microgel, as well as to a barely touching and a fully inter-penetrating pair, is shown in fig. S2. By using seven descriptors the contour is made much smoother while the main features of interest are preserved. With this method we sacrifice sharp corners but gain a more reliable measure of perimeters.

* Frank.Scheffold@unifr.ch

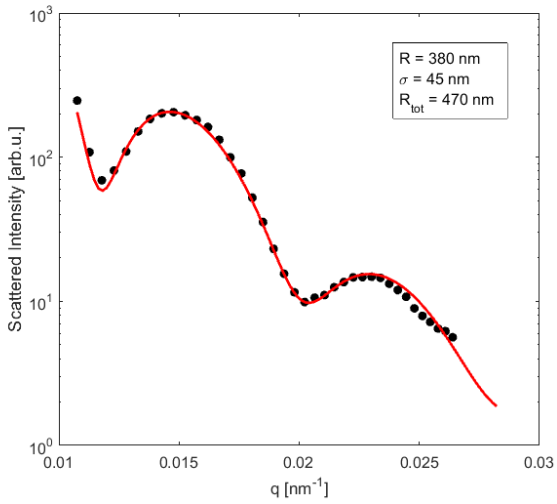

fig. S1. Form factor of pNIPAM microgels in dilute conditions. Measured (o) and (-) fit using the fuzzy sphere model. Fitting parameters are $R = 380\ nm$ and $\sigma = 45\ nm$, giving an overall particle size $R_{\rm tot} \simeq 470\ nm$ with a size polydispersity of 6%.

A. IsoQ vs Radius

To determine whether shape and size of particles are correlated quantities we calculate the Pearson correlation coefficient r between R and $IsoQ$, defined as $r_{R,IsoQ} = cov(R, IsoQ)/\sigma_R\sigma_{IsoQ}$ over the whole range of concentrations, as shown in fig. S3 (a). We also show in fig. S3 (b) the scatter plot of R versus $IsoQ$ for the lowest and highest concentrations of 10.6 wt% and 34 wt%. We find no clear sign of correlation. The scatter in the values obtained we attribute to sample heterogeneity and experimental error intrinsic to our measurement and analysis. While we cannot exclude a relation between size and deformability, it is likely that the resulting features are comparable to the noise in the contour which we are partially eliminating by smoothing.

B. Shape heterogeneity and number of facets

The shape and anisotropy of our 2D images of compressed microgels varies substantially from particle to particle. As an example we show in fig. S4 three different microgels at the highest concentration, having

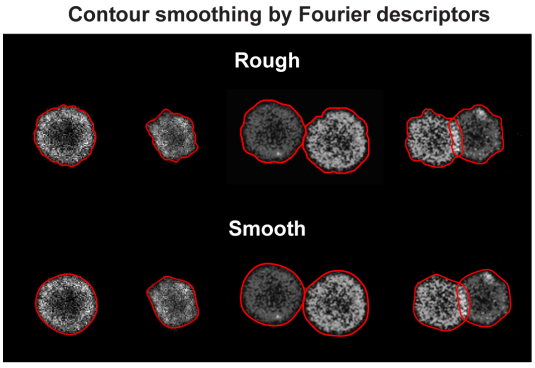

fig. S2. (Top) Rough contour obtained by Laplacian of Gaussian edge detection method (Bottom). Smooth contour obtained with seven Fourier descriptors.

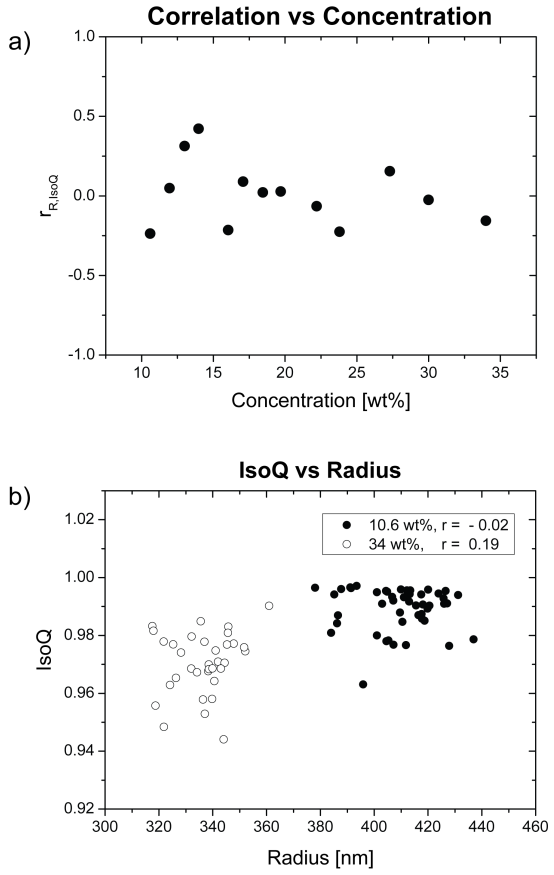

fig. S3. (a) Correlation coefficient r versus concentration (b). Scatter plots of R versus $IsoQ$ at 10.6 wt% and 34 wt%

different values of $IsoQ$. We characterize the shape heterogeneity in the final regime of particle compression ($c \geq 23.6$wt%), where facets can be clearly identified, in the following manner. We measure the curvature κ along the contour $r = (x, y)$ in cartesian coordinates, defined as $\kappa = |x'y'' - y'x''| / \left(x'^2 + y'^2\right)^{\frac{3}{2}}$. We then identify vertices of the particles as local maxima of curvature. The number of facets is equal to the number of vertices, while the experimental facet length L_{exp} is given by the distance between consecutive vertices. Two example images are shown in fig.S5.

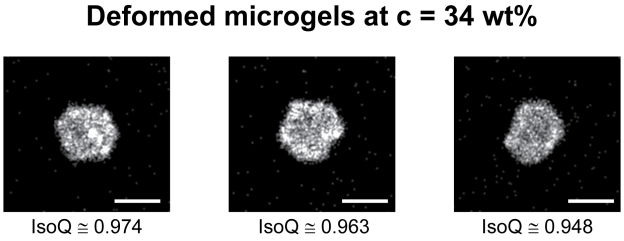

fig. S4. Sample images of deformed microgels at 34 wt% having different values of $IsoQ$. All scale bars are 500nm.

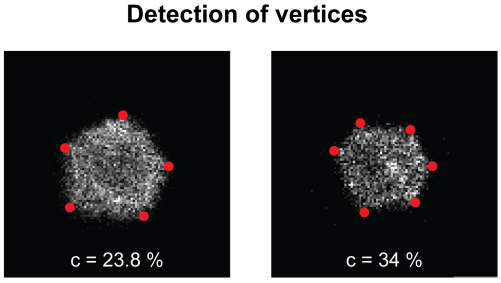

fig. S5. Vertices detected as maxima of curvature for deformed particles at different concentrations.

In Table S1 we report the average number of facets $\langle n \rangle$.

c [wt%]	23.8	27.3	30.5	34
$\langle n \rangle$	5.92 ± 0.65	6.09 ± 0.58	5.89 ± 0.56	5.96 ± 0.41

table S1. Average number of facets $\langle n \rangle$ as a function of concentration c in the final regime of isotropic compression.

Most particles have 6 facets and a few have 5 or 7. Larger numbers of facets are likely not detectable using our procedure due to the very weak curvature they would exhibit.

In order to quantify the heterogeneity in the detected polygon shapes we extract L_{exp} and compare it to the side length of a regular polygon L_{th}, having the same area A as the particle. For a regular polygon with n sides, such as a pentagon $n = 5$, hexagon $n = 6$ or heptagon $n = 7$, the side length is given by $L_{th} = \sqrt{\frac{4\,A\,tan(\pi/n)}{n}}$. An example for the distribution $P(L_{exp}/L_{\rm th})$ at a given concentration is shown in fig. S6.

Finally, we calculate the relative fluctuations of L_{exp}/L_{th} as a function of concentration. We find a mean value of roughly one in all cases and thus the heterogeneity in side length can be quantified by the standard deviation $\sigma_{L_{exp}/L_{th}}$. We find, on average, fluctuations of about 17%, with little change with increasing compression of the particles. The values, in percent, as a function of concentration are given in table S2.

In summary this supplementary data and analysis

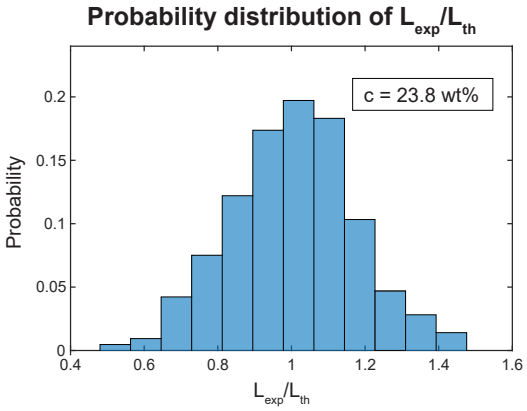

fig. S6. Distribution $P(L_{\text{exp}}/L_{\text{th}})$ at a concentration of 23.8 wt%

c [wt%]	23.8	27.3	30.5	34
$\sigma_{L_{exp}/L_{th}}$ [%]	17	18	16	16

table S2. Standard deviation of the distribution $P(L_{exp}/L_{\text{th}}$ characterizing the shape variation in the 2D images of microgels via the fluctuations of L_{exp}/L_{th}.

lends further evidence that shapes of the compressed particles remain unchanged in the final regime $c \geq 23.6$wt% while higher packing concentrations are achieved by isotropically compressing the polyhedral structures formed already at lower concentrations.

III. TWO-COLOR SUPERRESOLUTION MICROSCOPY - CALIBRATION PROCEDURE

Two-color experiments via spectral demixing are performed by placing an Optosplit II device (Cairn Research) before the camera. The device, schematically represented in fig. S7(a), houses a dichroic mirror (690 nm, AHF Analysentechnik, Germany) which partially splits the light emitted by the two fluorophores used, A647 and CF680, into short and long wavelength channels. Two lenses (L1, L2) and three mirrors (M1, M2, M3) serve to produce two spatially equivalent images side by side on the camera. To improve the spectral separation the mirror is slightly tilted to shift the edge wavelength closer to 700 nm. Calibration for color assignment and cross-talk determination is done as proposed by J. Schmoranzer et al. in the documentation for the SDmixer software (41). Samples containing only one dye species are prepared and 40,000 blinking frames are recorded for each, in the same conditions to be used in two-color imaging. Localization pairs are identified and used to populate intensity plots with coordinates given by the intensity in the short and long wavelength channels. The plots for both fluorophores serve as starting points

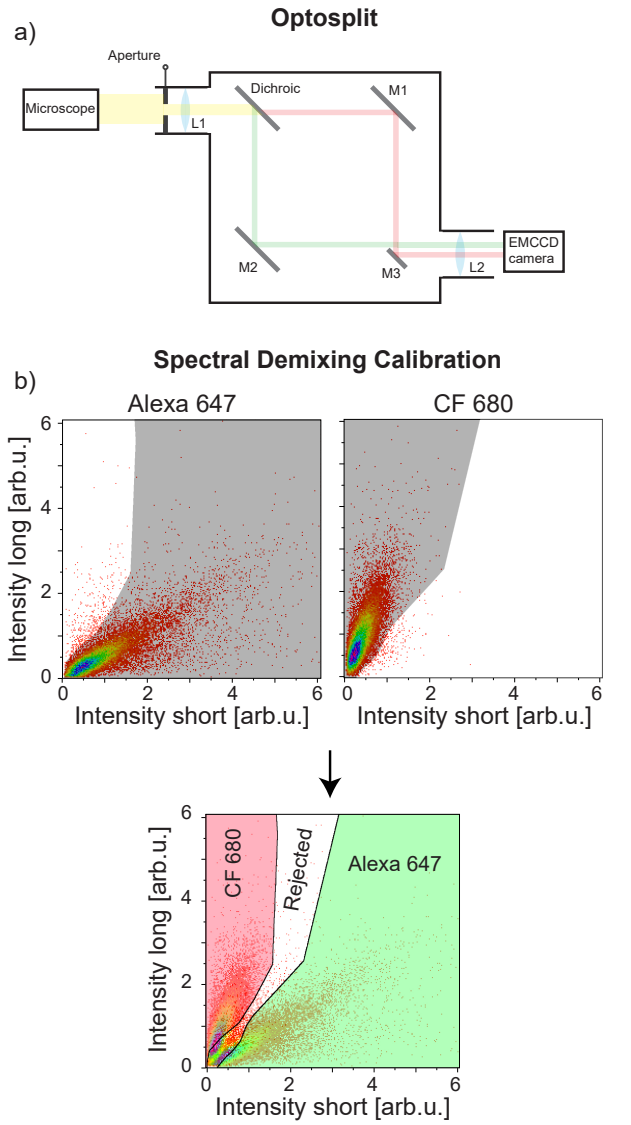

fig. S7. (a) Schematic representation of Optosplit used for two-color experiments. (b) Calibration measurements and filter design for color assignment after spectral demixing.

to design filters for color assignment, shown in fig.S7(b). The two fluorophores show distinct intensity distribu tions, A647 has higher intensity in the short wave length channel, and vice versa for CF680. The shaded areas are those assigned to the respective fluorophore while unshaded ones are excluded. The combined filters then show how localization pairs in a two-color experiment are assigned. Pairs falling in the green shaded area are assigned to A647, those in the red shaded area to CF680 and the rest are rejected. These filters are then used for all experiments. Cross-talk is measured as the percentage of pairs from one fluorophore falling in the area assigned to the other. From this calibration we obtain a cross-talk of 1%. The value depends both on the efficiency of spectral separation as well as on the design of the color assignment filters.